Photoelectrochemical C−H Activation of Methane to Methyl Radical at Room Temperature

SCHOLARONE™
Manuscripts

ARTICLE

Photoelectrochemical C–H Activation of Methane to Methyl Radical at Room Temperature

Fumiaki Amano,*[a] Ayami Shintani[b], Tatsuya Sakakura[c], Yoshiyuki Takatsuji[c], and Tetsuya Haruyama[c]

Herein, we report a continuous gas-fed photoelectrochemical (PEC) system with a proton exchange membrane for CH_4 activation at ambient temperature and pressure. We found that both water splitting and steam reforming of CH_4 were induced when the CH_4 concentration was low. O_2 and CO_2 were formed on titanium oxide (TiO_2) and tungsten trioxide (WO_3) photoanodes under ultraviolet light irradiation. We also found that visible light enhanced CH_4 activation and ethane (C_2H_6) formation. When the CH_4 concentration increased, O_2 formation was suppressed, with increasing production rates of CO_2, C_2H_6, and CO. Under optimised conditions, the selectivity of C_2H_6 reached 57% on a carbon basis over the WO_3 photoanode under visible-light irradiation. The production of C_2H_6 implies the formation of methyl radicals during the CH_4 gas-fed PEC process. We also demonstrated the PEC coupling of ethane to n-butane and the visible-light-induced oxidation of CH_4 without external bias.

Introduction

The catalytic conversion of CH_4 into value-added products is challenging because of its high stability and a large energy gap between its highest occupied and lowest unoccupied molecular orbitals.[1, 2] Moreover, its electron affinity is low (−1.9 eV),[3] the ionization potential (12.6 eV) and the C–H bond dissociation energy (439 kJ mol^{-1}) are high,[4] and the acidity is very weak (pK_a = 56).[5] The dipole moment of CH_4 is zero because of its symmetric structure. Therefore, high-temperature processes are typically used for catalytic CH_4 conversion. However, a low-temperature catalytic process may be promising for achieving high selectivity. Photoelectrochemical (PEC) reactions at room temperature differ from conventional catalytic processes.[6-10]

There are three pathways that convert CH_4 into methyl radicals ($\bullet CH_3$), as shown in Figure 1: electron transfer (ET), proton transfer (PT), and proton-coupled electron transfer (PCET). Among these reactions, ET ($CH_4 = \bullet CH_4^+ + e^-$, $\Delta_r G = 1163$ kJ mol^{-1}) and PT ($CH_4 = CH_3^- + H^+$, $\Delta_r G = 270$ kJ mol^{-1}) are extremely difficult to achieve. In contrast, PCET is more advantageous than stepwise transfer because the transfer of H^+ and e^- together can avoid the formation of high-energy chemical intermediates.[11-13] The $\Delta_r G$ of PCET ($CH_4 = \bullet CH_3 + H^+ + e^-$) is 198.7 kJ mol^{-1}. Thus, the potential of the $\bullet CH_3/CH_4$ couple is +2.06 V versus the standard hydrogen electrode (SHE).[7]

[a.] Department of Applied Chemistry for Environment, Tokyo Metropolitan University, 1-1 Minami-Osawa, Hachioji, Tokyo 192-0397, Japan
[b.] Department of Chemical and Environmental Engineering, The University of Kitakyushu, Kitakyushu, Fukuoka 808-0135, Japan
[c.] Department of Biological Functions and Engineering, Kyushu Institute of Technology, Kitakyushu, Fukuoka, 808-0196, Japan
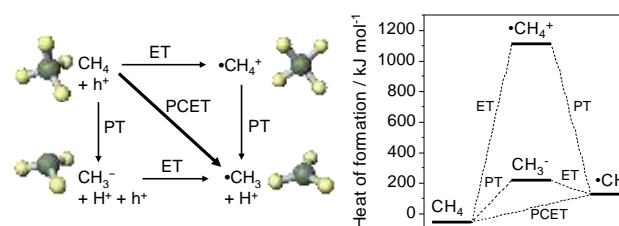
Figure 1. Activation of CH_4 to methyl radical through electron transfer (ET), proton transfer (PT), and proton-coupled electron transfer (PCET). The heat of formation was calculated by MOPAC PM3.
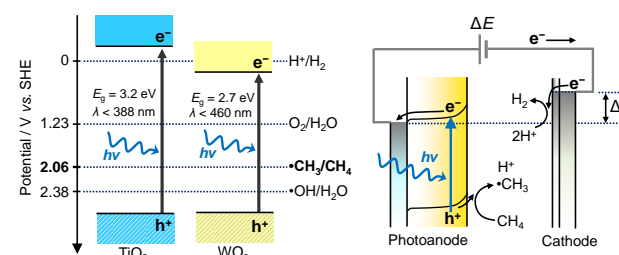

Figure 2. (a) Energy band diagram of TiO_2 and WO_3. (b) PEC process using photoanode and cathode under applied bias (ΔE).

The potential to form $\bullet CH_3$ is more negative than that for $\bullet OH/H_2O$ (+2.38 V vs. SHE). These potentials are suitable for titanium oxide (TiO_2) photocatalysts. Figure 2a shows the band diagram of anatase TiO_2, in which the valence band maximum (VBM) is located at approximately 3.0 V vs. SHE. Oxide semiconductors without partially filled d levels also exhibit a similar VBM.[14] Therefore, many semiconductor photocatalysts can activate CH_4 via the PCET mechanism. The nonoxidative coupling of methane (NOCM) is a well-known photocatalytic reaction ($2CH_4 \rightarrow C_2H_6 + H_2$, $\Delta G_{298K} = 68.6$ kJ mol^{-1}).[15, 16]
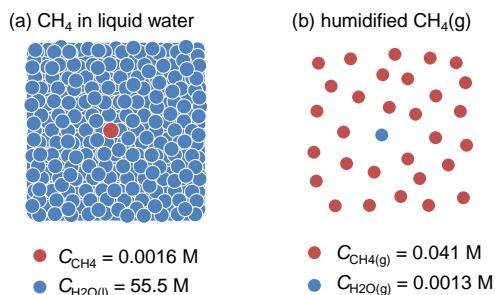
Figure 3. (a) Molar concentrations of (a) dissolved CH_4 and H_2O in liquid water, and (b) gaseous CH_4 and water vapor in humidified condition at 25°C.

However, the reported photocatalytic activities for NOCM are quite low.[17-24] In addition, TiO_2 can only use UV light as the band gap (E_g) of anatase TiO_2 is 3.2 eV.[25]

The PEC process can overcome the following limitations of TiO_2 photocatalysis: low activity and lack of visible-light sensitivity (Figure 2b). The external potential applied to the semiconductor electrodes improves the charge separation of the photoexcited carriers. Moreover, the applied voltage enables the use of visible light-responsive oxide semiconductors with a narrow E_g even though the conduction band minimum is too positive to induce the hydrogen evolution reaction (HER). Tungsten oxide (WO_3) photocatalysts are theoretically inactive for NOCM accompanied by HER, but the PEC process enables the HER on the cathode by applying voltages between the two electrodes.

Herein, we investigate the PEC process for CH_4 activation using TiO_2 and WO_3 photoanodes.[7-10, 26, 27] We developed a continuous gas-flow PEC reactor using a proton exchange membrane (PEM) as a solid electrolyte.[7, 28-30] The all-solid-state PEM-PEC cell is suitable for hydrophobic CH_4, which is insoluble in water. The maximum concentration of CH_4 is only 0.0016 M in water while that of water is 55.5 M in liquid (Figure 3).[4] However, in the case of humidified CH_4 gas, the saturated concentration of $H_2O(g)$ is 0.0013 M (3.16 kPa) at 25 °C, but the concentration of CH_4 is 0.041 M (101 kPa). We studied the probability of a gas-fed PEC process for CH_4 activation under both UV and visible-light irradiation.

Results and discussion

Photoanode materials and light wavelengths

CH_4 activation through PEC was tested using the PEM-PEC cell (Figure S1 in Electronic Supplementary Information, ESI) in a two-electrode system at 25 °C under atmospheric pressure. Figure 4 shows the time course of the PEC process using the TiO_2 and WO_3 photoanodes under a continuous flow of 10 vol% CH_4 and 3 vol% H_2O balanced with Ar. The cathode, which was separated from the photoanode using PEM, was a Pt/carbon electrocatalyst maintained under a humidified Ar flow. Humidification of the fed gases enhanced the proton conductivity of the PEM. The photoanode was irradiated with UV (365 nm) or blue light (453 nm). Before photoirradiation, the
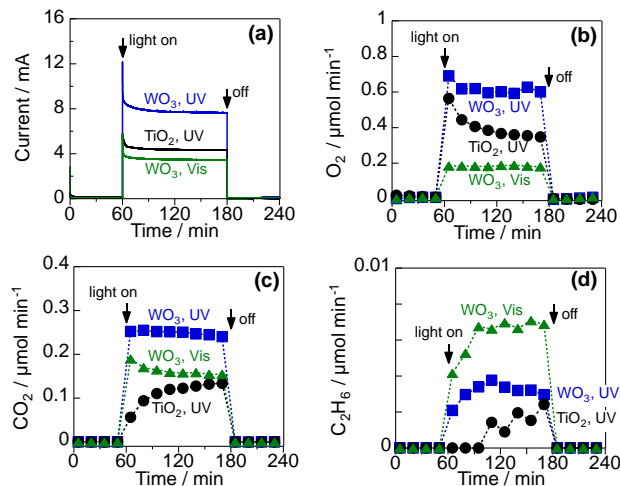

Figure 4. PEC activation of 10 vol% CH_4 using WO_3 and TiO_2 photoanodes under UV light (6.5 mW cm^{-2} at 365 nm) and visible light (6.8 mW cm^{-2} at 453 nm): (a) the overall current at 1.2 V, (b) the rate of O_2 evolution, (c) the rate of CO_2 formation, and (d) the rate of C_2H_6 formation on the photoanode side.

PEC system was kept in the dark to establish an adsorption–desorption equilibrium. Under irradiation, a good photocurrent response was observed for each condition when 1.2 V was applied between the photoanode and cathode catalysts (Figure 4a). The incident photon-to-current conversion efficiencies (IPCE) at steady state were 19.8% and 11.3% for the WO_3 and the TiO_2 photoanodes, respectively, at 365 nm. The IPCE at 453 nm was 8.4% for the WO_3 photoanode. This high quantum efficiency suggests efficient charge separation in the space-charge layer formed by the applied potential.

O_2, CO_2, and a small amount of C_2H_6 were obtained as products on the photoanodes (Figure 4b–d). Carbon monoxide could not be analysed under these conditions because of its interference with the Ar diluent. The production of O_2 and CO_2 suggests that both water vapour and CH_4 were oxidised on the photoanodes. The Faraday efficiencies (FE) of O_2 and CO_2 were approximately 50% and 40%, respectively, under UV irradiation for both photoanodes (Table S1 in ESI). The FE of O_2 decreased to 34% and that of CO_2 increased to 59% under visible-light irradiation of the WO_3 photoanode. The production rate of C_2H_6 also increased when 453-nm visible light was used instead of 365-nm UV light. These results suggest that CH_4 oxidation to CO_2 and C_2H_6 is more plausible than water oxidation under visible-light irradiation. The production of C_2H_6 implies that •CH_3 is generated by the PEC process; this is because the homocoupling of •CH_3 is involved in the formation mechanism of C_2H_6 in photo-Kolbe electrolysis.[31-33]

Methane concentration and light intensity

Figure 5 shows the effect of the concentration of CH_4 fed into the WO_3 photoanode under visible-light irradiation. The O_2 evolution rate decreased significantly when the CH_4 concentration increased to 50 vol%. The IPCE was 10.5%, and the FEs for O_2, CO_2, and C_2H_6 were 5.1%, 81.7%, and 4.9%, respectively (Table S2 in the ESI). For the cathode catalyst,
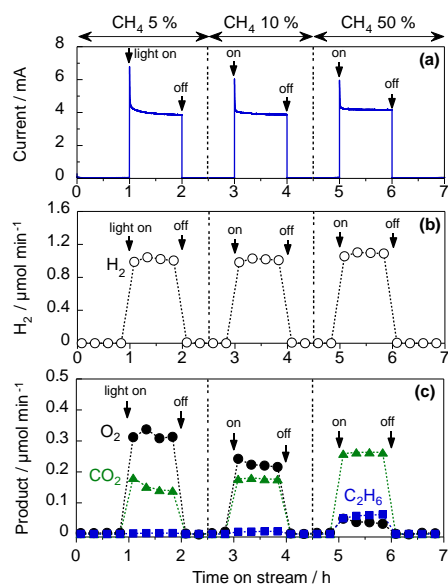
Figure 5. Effect of CH₄ concentration on the PEC reactions over the WO₃ photoanode:(a) the overall current at 1.2 V, (b) the rate of H_2 evolution on the cathode side, and (c) the rate of products formation on the photoanode side under visible-light irradiation (6.8 mW cm⁻² at 453 nm).
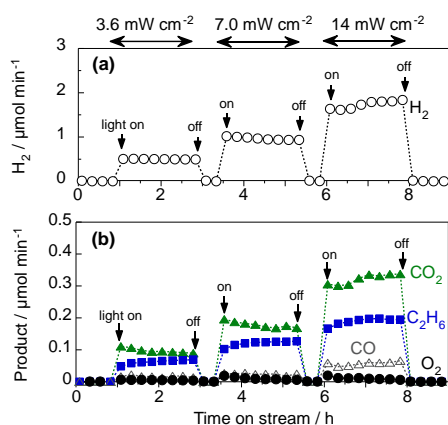

Figure 6. Effect of light intensity on the activation of humidified CH₄ using the WO₃ photoanode under 453-nm irradiation at 1.2 V; (a) the H_2 evolution rate on the cathode side and (c) the rates of product formation on the photoanode side.

stoichiometric H_2 evolution (FE of ~100%) was observed, indicating that the steam reforming of methane ($CH_4 + 2H_2O_{(g)} \rightarrow CO_2 + 4H_2$) was mainly promoted in this PEM-PEC reactor. To the best of our knowledge, this is the first report of the gas-fed PEC steam reforming of methane, which is an uphill reaction (ΔG_{298K} = 114 kJ mol⁻¹).[15, 16] Notably, the purity of the evolved H_2 can be sustained by the membrane separation from CH₄ and the oxidised products. The H_2 production rate, and thus the photocurrent, did not depend on the CH₄ concentration, suggesting that the charge-separation efficiency was determined by the applied potential rather than the surface reactions.

Figure 6 shows the PEC properties of the WO₃ photoanode under the flow of 97 vol% CH₄ and 3 vol% H_2O vapour.[7] When the light intensity is 3.6 mW cm⁻², the FEs of O_2, CO_2, CO, and

C_2H_6 were 1.5%, 72.3%, 8.3%, and 14.0%, respectively. The sum of the FE values was 96%, suggesting that unidentified products were limited, and no methanol was formed. The FE of C_2H_6 was not very high because only two electrons were donated from CH₄ to produce a C_2H_6 molecule and eight electrons produced a CO_2 molecule. From the viewpoint of selectivity, the production rate of C_2H_6 was comparable to that of CO_2 at high CH₄ concentrations and low light intensities. The C_2H_6 selectivity on a carbon basis reached 57.4%, whereas the selectivities for CO_2 and CO were 37.0% and 5.6%, respectively (Table S3 in the ESI). This indicates that more than half of the PEC process can be explained by the dehydrogenative coupling of methane, similar to photocatalytic NOCM.[7]

The high C_2H_6 selectivity implies the efficient formation of •CH₃ by the photogenerated holes of WO₃. When the concentration of the generated •CH₃ is high, homocoupling should easily occur to produce C_2H_6. In contrast, other side reactions of •CH₃ are promoted, thereby decreasing C_2H_6 selectivity at low CH₄ concentrations.

The production rates of CO_2, CO, and C_2H_6 increased with the incident light intensity (Figure 6). This indicated that the products were formed via the photoexcitation mechanism. The C_2H_6 selectivity gradually decreased from 57.4% to 49.1% when the irradiance intensity was changed from 3.6 to 14 mW cm⁻², implying that overoxidation is promoted when the concentration of holes is high at the semiconductor surface. Although the photocurrent fluctuated over time, which may have been affected by humidity, the WO₃ photoanode repeatedly exhibited sufficient stability for several hours. We also did not confirm the degradation of the crystallinity of WO₃ or the structure of the ionomer coated on the photoanode surface, as shown in X-ray diffraction patterns (Figure S2) and Fourier transform infrared spectra (Figure S3).

PEC reaction mechanism

To further investigate the radical mechanism of the PEC process, we tested the PEC oxidation of C_2H_6.[34] Figure 7 shows the time course of the C_2H_6 activation on the WO₃ photoanode. We detected *n*-butane as the product. The
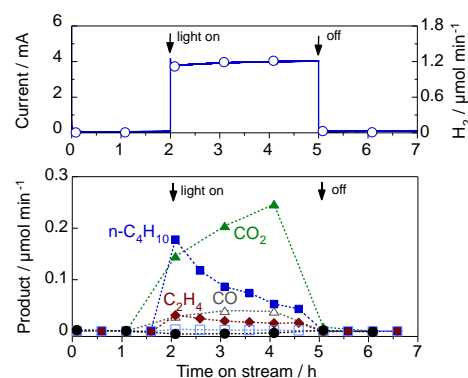

Figure 7. PEC activation of C_2H_6 using WO₃ photoanode under visible-light irradiation (6.8 mW cm⁻² at 453 nm) at 1.2 V; (a) the overall current and H_2 evolution rate on the cathode side, and (b) the rates of product formation on the photoanode side.
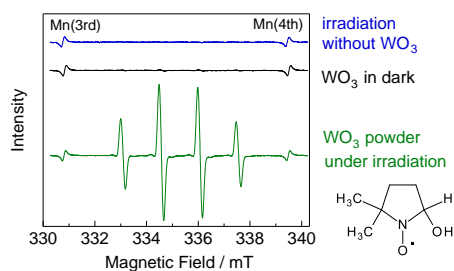
Figure 8. EPR spectra of an aqueous solution of DMPO and $AgNO_3$ after 405-nm irradiation for 5 min without WO_3 powder, aging in the dark with WO_3 powder, and 405-nm irradiation for 5 min with WO_3 powder. The standard Mn^{2+} marker shows signals at g = 2.0337 (third line) and g = 1.9803 (fourth line).

formation of n-butane suggests the occurrence of the homocoupling of ethyl radicals ($\bullet C_2H_5 + \bullet C_2H_5 \rightarrow CH_3\text{-}CH_2\text{-}CH_2\text{-}CH_3$). We also detected the formation of ethylene, which could have been generated through intermolecular dehydrogenation ($C_2H_6 + 2h^+ \rightarrow CH_2=CH_2 + 2H^+$). The FE of *n*-butane was 4.4%, and its selectivity was 39.7% (C-basis), as shown in Table S4 in the ESI.

To investigate the radical intermediates involved in the activation of CH_4, we conducted electron paramagnetic resonance (EPR) experiments using 5,5-dimethyl-1-pyrroline-N-oxide (DMPO) as a spin-trapping agent.[35] Photoirradiation was performed for WO_3 powder dispersed in a 50 mM $AgNO_3$ aqueous solution with CH_4 gas. The silver cation acted as an electron acceptor for the photoexcited WO_3.[36] We observed four-line EPR signals (g = 2.0056, A_N = 1.49 mT, A_H = 1.49 mT), which were consistent with the $\bullet$DMPO-OH spin adduct in the WO_3 suspension after irradiation (Figure 8). This implied that $\bullet$OH could form on the WO_3 photoanode in the presence of water vapour. Therefore, $\bullet$OH was the active species for CH_4 activation in the PEM-PEC system. In contrast, we could not detect a signal corresponding to the $\bullet$DMPO-CH_3 spin adduct, even in the presence of acetic acid and dimethyl sulfoxide. This suggests that spin trapping of $\bullet CH_3$ with DMPO is difficult in liquid water under our experimental conditions.

We also attempted a photo-Kolbe reaction using WO_3 powder, 5 vol% acetic acid, and 50 mM $AgNO_3$.[33, 36] The gaseous products obtained were CO_2, CH_4, and O_2 (Figure S4 in ESI). A trace amount of methanol was also formed in the aqueous solution. However, C_2H_6 was not formed in the aqueous system, indicating the importance of the vapour-fed conditions in C_2H_6 production.

The advantage of the gas-fed type reactor was also revealed by the gas flow rate dependence of C_2H_6 formation (Figure S5 in ESI). The production rate of C_2H_6 was very low at a gas flow rate of 1 mL min^{-1}. We realised that gas diffusion plays an important role in C_2H_6 production in the PEM-PEC system because productivity increased at higher flow rates. The proposed reaction mechanism for the catalytic oxidative coupling of methane involves the coupling of $\bullet CH_3$ in the gas phase to form C_2H_6.[2, 37] Similar to this mechanism, continuous flow facilitates the desorption of $\bullet CH_3$ from the surface of the WO_3 photoanode and the formation of C_2H_6.
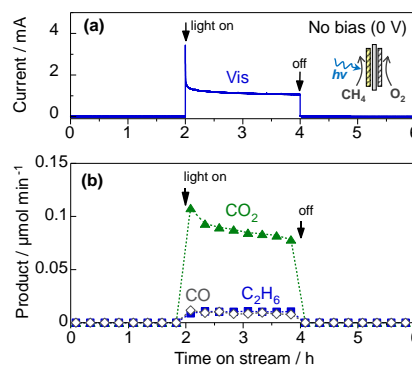

Figure 9. PEC oxidation of CH_4 by the PEM-PEC reactor using the WO_3 photoanode and Pt/carbon catalyst: (a) the overall current at zero bias, and (b) the rate of products formation on the photoanode side under 453-nm light irradiation (6.8 mW cm^{-2}).

Zero-bias PEC oxidation of methane

The photocatalytic oxidation of atmospheric CH_4 to CO_2 is another attractive reaction because the greenhouse gas effect of CH_4 is over 30 times greater than that of CO_2. The complete oxidation of methane is an exergonic reaction ($CH_4 + 2O_2 \rightarrow CO_2 + 2H_2O(g)$, ΔG_{298K} = −801 kJ mol^{-1}),[15, 16] but its high activation energy prevents the catalytic reaction at room temperature.

Figure 9 shows the PEC oxidation of CH_4 in the PEM-PEC reactor using the WO_3 photoanode under blue-light irradiation at 25 °C. CO_2 formation by CH_4 oxidation was confirmed without an external bias voltage. During the exergonic reaction, the oxygen reduction reaction ($O_2 + 4H^+ + 4e^- = H_2O$, 1.23 V vs. SHE) was promoted over the Pt/carbon catalyst in humidified air (Figure 2a). The IPCE at zero bias was 2.5% at 453 nm, which was much higher than the quantum efficiency previously reported for photocatalytic systems.[38, 39]

Experimental

Preparation of photoanodes.

Ti felt was used as the conductive substrate for the gas-diffusion photoanodes. The WO_3 electrode was prepared by dip coating with an aqueous solution of $(NH_4)_6H_2W_{12}O_{40}$ and polyethylene glycol; the electrode was then calcined at 923 K for 2 h.[7, 28, 40] The TiO_2 electrode was prepared by the anodization of Ti felt in ethylene glycol with 0.25 wt% NH_4F and 10 vol% H_2O at 50 V for 3 h.[29, 41, 42] The anodized Ti felt was calcined at 823 K for 1 h to crystallize into anatase TiO_2. The photoanodes were modified using a Nafion ionomer dispersion (Sigma-Aldrich).

PEM-PEC reaction

The PEC measurements were performed at 25 °C and 1 bar using an AMETEK VersaSTAT3 workstation. For the proposed all-solid-state cells, a Nafion N117 film (DuPont) was sandwiched between the photoanode and the cathode, which was composed of Pt/carbon (Tanaka Kikinzoku Kogyo) and Toray carbon paper (Fuel Cell Store). The photoanode side was

supplied with 20 mL min^{-1} of humidified CH$_4$/Ar or humidified CH$_4$ gas. The relative humidity was approximately 90% without liquid condensation. The cathode side was supplied with 20 mL min^{-1} of humidified Ar gas. The geometric surface areas of the two electrodes were 25 cm^2, whereas that of the photoanode was 16 cm^2. Photoirradiation was performed through a glass window using light-emitting diodes (LED). The peak wavelengths were 365 and 453 nm for the UV (Nitride Semiconductor) and blue LED (OptoSupply), respectively. The IPCE was calculated as follows:

$$\text{IPCE} = \frac{1240 j_{\text{photo}}}{\lambda I_0} \times 100\%$$

Here, j_{photo} is the photocurrent density, λ is the wavelength (nm), and I_0 is the intensity of incident light.

Product analysis

The gas products of the PEC reaction were analysed using gas chromatography (Shimadzu GC-8A and GC-2014). A thermal conductivity detector (TCD) equipped with a molecular sieve 5A column in an Ar carrier was used to quantify H$_2$ and O$_2$. A TCD with a Shincarbon ST column in an He carrier was used to quantify CO and CO$_2$. A flame ionisation detector with a GS-CarbonPLOT was used to detect alkane species.

The C$_2$H$_6$ selectivity in carbon basis was calculated using the below equation:

$$S_{\text{C2H6}} = \frac{2r_{\text{C2H6}}}{r_{\text{CO2}} + r_{\text{CO}} + 2r_{\text{C2H6}}} \times 100\%$$

Here, r_i is the production rate of each carbon-containing product determined by online GC and is referenced to the calibration curves from the standard gas sample. The corresponding FE values are calculated as follows:

$$\text{FE} = \frac{n_i F r_i}{j_{\text{photo}}} \times 100\%$$

Here, n_i is the number of electrons involved, and F is the Faradaic constant. The n_i values for C$_2$H$_6$, O$_2$, CO, and CO$_2$ are 2, 4, 6, and 8, respectively.

Characterization

X-ray diffraction patterns were recorded by a Rigaku SmartLab diffractometer using Cu Kα radiation. Fourier transform infrared spectroscopy was performed on a Shimadzu IR Affinity-1 spectrometer in the attenuated total reflection mode. Electron paramagnetic resonance (EPR) spectra were recorded using a JES-X310 spectrometer (JEOL, Japan) at room temperature. The sample suspension was taken out by a quartz capillary tube with the two ends sealed by sealing compound for the EPR measurement.

Conclusions

We studied the PEC activation of CH$_4$ over TiO$_2$ and WO$_3$ photoanodes in a gas-flow PEM-PEC system. We demonstrated

that a WO$_3$ photoanode excited by visible light converts CH$_4$ into CO$_2$ and C$_2$H$_6$. At high CH$_4$ concentrations, the C$_2$H$_6$ selectivity was above 50% on a carbon basis. Moreover, we found that WO$_3$ and visible light were more suitable than TiO$_2$ and UV light to form C$_2$H$_6$. When C$_2$H$_6$ was used as the reactant, n-butane was formed, suggesting a radical coupling mechanism. The WO$_3$ photoanode showed an IPCE of 7.6% at 453 nm with an applied voltage of 1.2 V. The current efficiency of H$_2$ was nearly 100% in the cathode compartment, demonstrating that the PEM-PEC system is useful for steam reforming of methane and dehydrogenative methane coupling. Surprisingly, visible-light induced CH$_4$ oxidation was also efficiently promoted in the PEM-PEC system using humidified air, even under zero bias.

Author Contributions

Fumiaki Amano: Conceptualisation, Methodology, Validation, Visualisation, Writing - Review & Editing, and Supervision. Ayami Shintani: Investigation Visualisation, and Writing - Original Draft. Tatsuya Sakakura and Yoshiyuki Takatsuji: Investigation. Tetsuya Haruyama: Validation and Resources.

Conflicts of interest

There are no conflicts to declare.

Acknowledgements

Notes and references

1. K. Yoshizawa, *Acc. Chem. Res.*, 2006, **39**, 375-382.
2. P. Schwach, X. Pan and X. Bao, *Chem. Rev.*, 2017, **117**, 8497-8520.
3. C.-G. Zhan, J. A. Nichols and D. A. Dixon, *J. Phys. Chem. A*, 2003, **107**, 4184-4195.
4. J. R. Rumble, *CRC handbook of chemistry and physics*, CRC Press, Boca Raton, 100th edn., 2019.
5. F. G. Bordwell, *Acc. Chem. Res.*, 1988, **21**, 456-463.
6. J. Baltrusaitis, I. Jansen and J. D. Schuttlefield Christus, *Catal. Sci. Technol.*, 2014, **4**, 2397-2411.
7. F. Amano, A. Shintani, K. Tsurui, H. Mukohara, T. Ohno and S. Takenaka, *ACS Energy Lett.*, 2019, **4**, 502-507.
8. J. Ma, K. K. Mao, J. X. Low, Z. H. Wang, D. W. Xi, W. Q. Zhang, H. X. Ju, Z. M. Qi, R. Long, X. J. Wu, L. Song and Y. J. Xiong, *Angew. Chem. Int. Ed.*, 2021, **60**, 9357-9361.
9. A. Mehmood, S. Y. Chae and E. D. Park, *Catalysts*, 2021, **11**, 1387.
10. H. Tateno, S. Iguchi, Y. Miseki and K. Sayama, *Angew. Chem. Int. Ed.*, 2018, **57**, 11238-11241.
11. J. J. Warren, T. A. Tronic and J. M. Mayer, *Chem. Rev.*, 2010, **110**, 6961-7001.
12. J. N. Schrauben, R. Hayoun, C. N. Valdez, M. Braten, L. Fridley and J. M. Mayer, *Science*, 2012, **336**, 1298-1301.

13.   H. Schwarz, S. Shaik and J. L. Li, *J. Am. Chem. Soc.*, 2017, **139**, 17201-17212.
14.   D. E. Scaife, *Solar Energy*, 1980, **25**, 41-54.
15.   H. Yokokawa, S. Yamauchi and T. Matsumoto, *Calphad*, 1999, **23**, 357-364.
16.   W. H. E. D. D. Wagman, V. B. Parker, R. H. Schumm, I. Halow, S. M. Bailey, K. L. Churney, R. L. Nuttall, *J. Phys. Chem. Ref. Data* 1982, **11**, Supplement No.2.
17.   L. Yuliati, T. Hattori, H. Itoh and H. Yoshida, *J. Catal.*, 2008, **257**, 396-402.
18.   K. Shimura and H. Yoshida, *Catal. Surv. Asia*, 2014, **18**, 24-33.
19.   L. Yu and D. Li, *Catal. Sci. Technol.*, 2017, **7**, 635-640.
20.   S. Q. Wu, X. J. Tan, J. Y. Lei, H. J. Chen, L. Z. Wang and J. L. Zhang, *J. Am. Chem. Soc.*, 2019, **141**, 6592-6600.
21.   S. Q. Wu, L. Z. Wang and J. L. Zhang, *J. Photochem. Photobiol. C*, 2021, **46**, 100400.
22.   S. P. Singh, A. Anzai, S. Kawaharasaki, A. Yamamoto and H. Yoshida, *Catal. Today*, 2021, **375**, 264-272.
23.   S. P. Singh, A. Yamamoto, E. Fudo, A. Tanaka, H. Kominami and H. Yoshida, *ACS Catal.*, 2021, **11**, 13768-13781.
24.   L. Li, G.-D. Li, C. Yan, X.-Y. Mu, X.-L. Pan, X.-X. Zou, K.-X. Wang and J.-S. Chen, *Angew. Chem. Int. Ed.*, 2011, **50**, 8299-8303.
25.   W. Q. Zhang, C. F. Fu, J. X. Low, D. L. Duan, J. Ma, W. B. Jiang, Y. H. Chen, H. J. Liu, Z. M. Qi, R. Long, Y. F. Yao, X. B. Li, H. Zhang, Z. Liu, J. L. Yang, Z. G. Zou and Y. J. Xiong, *Nature Commun.*, 2022, **13**, 2806.
26.   W. Li, D. He, G. Hu, X. Li, G. Banerjee, J. Li, S. H. Lee, Q. Dong, T. Gao, G. W. Brudvig, M. M. Waegele, D.-e. Jiang and D. Wang, *ACS Cent. Sci.*, 2018, **4**, 631-637.
27.   S. J. Xie, Z. B. Shen, J. Deng, P. Guo, Q. H. Zhang, H. K. Zhang, C. Ma, Z. Jiang, J. Cheng, D. H. Deng and Y. Wang, *Nature Commun.*, 2018, **9**.
28.   F. Amano, A. Shintani, H. Mukohara, Y. M. Hwang and K. Tsurui, *Front. Chem.*, 2018, **6**, 598.
29.   F. Amano, H. Mukohara, A. Shintani and K. Tsurui, *ChemSusChem*, 2019, **12**, 1925-1930.
30.   F. Amano, H. Mukohara, H. Sato, C. Tateishi, H. Sato and T. Sugimoto, *Sustain. Energy Fuels*, 2020, **4**, 1443-1453.
31.   B. Kraeutler and A. J. Bard, *J. Am. Chem. Soc.*, 1977, **99**, 7729-7731.
32.   B. Kraeutler, C. D. Jaeger and A. J. Bard, *J. Am. Chem. Soc.*, 1978, **100**, 4903-4905.
33.   S. Sato, *J. Phys. Chem.*, 1983, **87**, 3531-3537.
34.   S. P. Singh, A. Yamamoto and H. Yoshida, *Catal. Sci. Technol.*, 2022, **12**, 1551-1561.
35.   M. H. Ab Rahim, M. M. Forde, R. L. Jenkins, C. Hammond, Q. He, N. Dimitratos, J. A. Lopez-Sanchez, A. F. Carley, S. H. Taylor, D. J. Willock, D. M. Murphy, C. J. Kiely and G. J. Hutchings, *Angew. Chem. Int. Ed.*, 2013, **52**, 1280-1284.
36.   T. Sakata, T. Kawai and K. Hashimoto, *J. Phys. Chem.*, 1984, **88**, 2344-2350.
37.   B. L. Farrell, V. O. Igenegbai and S. Linic, *ACS Catal.*, 2016, **6**, 4340-4346.
38.   J. Zhang, Y. Wang, Y. Wang, Y. Bai, X. Feng, J. Zhu, X. Lu, L. Mu, T. Ming, R. de Richter and W. Li, *Chem. Eur. J.*, 2022, **28**, e202201984.
39.   X. Chen, Y. Li, X. Pan, D. Cortie, X. Huang and Z. Yi, *Nature Commun.*, 2016, **7**, 12273.
40.   F. Amano, A. Shintani, K. Tsurui and Y.-M. Hwang, *Mater. Lett.*, 2017, **199**, 68-71.
41.   M. V. Makarova, F. Amano, S. Nomura, C. Tateishi, T. Fukuma, Y. Takahashi and Y. E. Korchev, *ACS Catal.*, 2022, **12**, 1201-1208.
42.   F. Amano, S. Nomura, C. Tateishi and S. Nakayama, *J. Electrochem. Soc.*, 2023, **170**, 026501.